

Integrated high electron mobility transistors in GaAs/AlGaAs heterostructures for amplification at sub-Kelvin temperatures

Cite as: Appl. Phys. Lett. **114**, 053104 (2019); <https://doi.org/10.1063/1.5083818>

Submitted: 30 November 2018 . Accepted: 21 January 2019 . Published Online: 05 February 2019

L. A. Tracy, J. L. Reno, S. Fallahi, and M. J. Manfra



View Online



Export Citation



CrossMark

ARTICLES YOU MAY BE INTERESTED IN

[Thermophotonic cooling in GaAs based light emitters](#)

Applied Physics Letters **114**, 051101 (2019); <https://doi.org/10.1063/1.5064786>

[AlGaIn polarization-doped field effect transistor with compositionally graded channel from \$\text{Al}_{0.6}\text{Ga}_{0.4}\text{N}\$ to AlN](#)

Applied Physics Letters **114**, 052103 (2019); <https://doi.org/10.1063/1.5058263>

[Robust quantum anomalous Hall effect with electrically tunable band gap in Ta-decorated silicene](#)

Applied Physics Letters **114**, 053105 (2019); <https://doi.org/10.1063/1.5065789>

Applied Physics Reviews
Now accepting original research

2017 Journal
Impact Factor:
12.894



Integrated high electron mobility transistors in GaAs/AlGaAs heterostructures for amplification at sub-Kelvin temperatures

Cite as: Appl. Phys. Lett. **114**, 053104 (2019); doi: [10.1063/1.5083818](https://doi.org/10.1063/1.5083818)

Submitted: 30 November 2018 · Accepted: 21 January 2019 ·

Published Online: 5 February 2019



View Online



Export Citation



CrossMark

L. A. Tracy,^{1,a)} J. L. Reno,² S. Fallahi,³ and M. J. Manfra^{3,4,5}

AFFILIATIONS

¹Sandia National Laboratories, Albuquerque, New Mexico 87185, USA

²Center for Integrated Nanotechnologies, Sandia National Laboratories, Albuquerque, New Mexico 87185, USA

³Department of Physics and Astronomy and Birck Nanotechnology Center, Purdue University, West Lafayette, Indiana 47907, USA

⁴School of Materials Engineering and Birck Nanotechnology Center, Purdue University, West Lafayette, Indiana 47907, USA

⁵School of Electrical and Computer Engineering, Purdue University, West Lafayette, Indiana 47907, USA

^{a)}Electronic mail: latracy@sandia.gov

ABSTRACT

We demonstrate the use of custom high electron mobility transistors (HEMTs) fabricated in GaAs/AlGaAs heterostructures to amplify current from quantum dot devices. The amplifier circuit is located adjacent to the quantum dot device, at sub-Kelvin temperatures, in order to reduce the impact of cable capacitance and environmental noise. Using this circuit, we show a current gain of 380 for 0.56 μ W of power dissipation, with a bandwidth of 2.7 MHz and current noise referred to the input of 24 fA/Hz^{1/2} for frequencies of 0.1–1 MHz. The power consumption required for similar gain is reduced by more than a factor of 20 compared to a previous demonstration using a commercial off-the-shelf HEMT. We also demonstrate integration of a HEMT amplifier circuit on-chip with a quantum dot device, which has the potential to reduce parasitics and should allow for more complex circuits with reduced footprints.

Published under license by AIP Publishing. <https://doi.org/10.1063/1.5083818>

Spins in semiconductors are a promising platform for quantum computing.^{1–5} High fidelity single qubit control^{6–10} and single shot readout^{11–14} have already been demonstrated in various semiconductor spin qubit systems. Here, we focus, in particular, on the readout of spin qubits using spin-to-charge conversion and sensing of the resulting change in the charge configuration with a quantum dot or quantum point contact.^{3,15} This readout method requires detection of a change in resistance of a charge sensor, where the resulting current or voltage signal is typically small and originates from the lowest temperature stage of a dilution refrigerator. A variety of approaches exist for detection of this signal, including RF reflectometry,^{16–18} Josephson parametric amplification,¹⁹ and direct amplification using cryogenic transistors.^{20–24} However, room still exists for improvement in terms of simplifying readout techniques (e.g., possibly avoiding the need for resonators and bulky microwave components such as circulators²⁵) and a further increase in the speed and fidelity

of single shot readout is desirable for quantum error correction protocols.^{26,27}

Recent experiments have shown improvements in spin qubit readout using commercial off-the-shelf semiconductor-based [high electron mobility transistor (HEMT) or heterojunction bipolar transistor] amplifiers located adjacent to the qubit chip, mounted on the mixing chamber stage of a dilution refrigerator.^{23,24} This approach mitigates the impact of cable capacitance and environmental noise such as triboelectric noise in cabling. In this article, we show further improvements in this approach by the use of custom HEMTs fabricated in GaAs/AlGaAs heterostructures supporting high mobility two-dimensional electron systems. The custom HEMT amplifier is located adjacent to the quantum dot device, either on an adjacent die or fully integrated on the same die with the quantum dot, in both cases operating at sub-Kelvin temperatures.

In this article, we present data for two different devices. For the first device (device A—not shown), the HEMT is located on a separate die, separated by a few mm, from the quantum dot and passives (resistors and capacitor). In this case, a 1 mil Au wire bond connects the HEMT gate to capacitor C1. For the second device (device B), the HEMT, passives, and quantum dot are all located on the same die as shown in Fig. 1(a). The quantum dot device has a similar layout and dimensions to the charge sensor dots shown in Refs. 28 and 29. Resistors and capacitors for the amplifier circuit are fabricated on-chip. Capacitor C1 is a metal-insulator-metal structure consisting of an initial Ti (10 nm)/Au (200 nm)/Ti (10 nm) metal layer, an Al_2O_3 dielectric (50 nm) deposited via atomic layer deposition, and a Ti (10 nm)/Au (200 nm) top metal layer. Resistors R1 and R2 are thin film meander line structures consisting of a 20 nm thick layer of nichrome with a sheet resistance of $\sim 100 \Omega/\text{sq}$, evaporated from an 80:20 NiCr alloy source.

A diagram of the HEMT amplifier circuit is shown in Fig. 1(c). This circuit is similar to the one utilized in Ref. 24, except that in this case only a single transistor amplification stage is used. Current through the dot is converted to voltage by resistor R2, which is chosen to be comparable to or less than typical quantum dot resistances ($\sim 100 \text{ k}\Omega$). Capacitor C1 allows AC coupling of this voltage to the HEMT gate, while the DC HEMT gate voltage (V_g) is set by the bias on resistor R1, as indicated in Fig. 1(c). The HEMT source is connected to a room temperature bias tee with the DC port grounded and the RF port connected to a room temperature transimpedance amplifier.

Devices are fabricated using Si modulation doped GaAs/AlGaAs heterostructures containing a two-dimensional electron gas (2DEG) formed by a single interface heterojunction, as sketched in Fig. 1(b). For device A, the 2DEG is located 92 nm

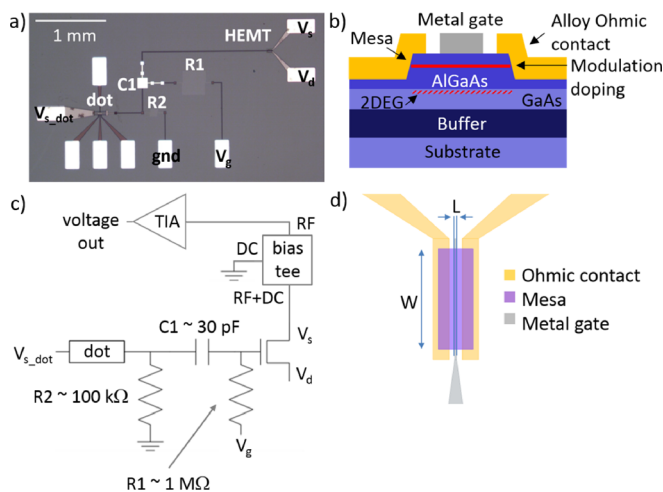


FIG. 1. (a) Optical image of the integrated HEMT amplifier device (device B), showing quantum dots, capacitor C1, resistors R1 and R2, and HEMT, located on a single die. (b) Sketch of the cross-section of the HEMT device (not to-scale) showing the mesa region with the 2DEG, metal gate, and Ohmic contacts. (c) Diagram of the HEMT amplifier circuit. (d) Top-down sketch of the HEMT device (not to-scale), showing the metal gate with length L and width W .

below the surface and has an as-grown density of $1.3 \times 10^{11} \text{ cm}^{-2}$ and a low-temperature ($T = 300 \text{ mK}$) mobility of $2.3 \times 10^6 \text{ cm}^2/\text{Vs}$, while for device B, the 2DEG is located 57 nm below the surface and has an as-grown density of $2.5 \times 10^{11} \text{ cm}^{-2}$ and a mobility of $3.3 \times 10^6 \text{ cm}^2/\text{Vs}$, also measured at $T = 300 \text{ mK}$. Cross-sectional and top-down diagrams of the HEMT are shown in Figs. 1(b) and 1(d), respectively. As indicated in Figs. 1(b) and 1(d), the HEMT device consists of a mesa region containing a 2DEG, Ohmic contacts to form the HEMT source and drain, and a metal gate (TiAu) with width W and length L . For devices A and B, the gate length and width are $L = 0.5 \mu\text{m}$ and $W = 400 \mu\text{m}$ and $L = 3 \mu\text{m}$ and $W = 70 \mu\text{m}$, respectively. NiAuGe alloy Ohmic contacts are formed by evaporating 4 nm Ni, 120 nm Au, 60 nm Ge, and 40 nm Ni and annealing in forming gas at 440°C for 10 min.

For low temperature characterization, samples were mounted on the cold finger of a dilution refrigerator. The die is attached to a gold plated copper layer of a printed circuit board using Apiezon N grease, where the copper layer is in good thermal contact with the dilution refrigerator cold finger. Stainless steel semi-rigid coaxial lines are used for the HEMT source and drain and dot device source connections. The center conductor of these coaxial lines is thermalized at each temperature stage through ceramic heatsinks with a microstrip geometry. Resistive twisted pair wiring with low-temperature low pass filtering (1 kHz cutoff frequency) is used for all other connections.

We first focus on the DC transport characteristics of the HEMT devices for mixing chamber temperatures $T_{MC} < 100 \text{ mK}$, as shown in Fig. 2. To minimize power dissipation, the HEMTs are operated at a low source-drain bias ($< 0.1 \text{ V}$) and at gate voltages very close to threshold. For example, the white cross in Fig. 2(a) indicates an optimal bias point for operation with a power consumption of $0.56 \mu\text{W}$. The total contact resistance (source and drain) for both devices was less than 50Ω so that the transport characteristics shown in Fig. 2 are dominated by the 2DEG channel. Comparing Figs. 2(a) and 2(b), differences in transport can be seen for the two HEMTs with different gate dimensions. In terms of amplifier performance, the most significant difference is that the transconductance, dI_D/dV_{GS} , is larger for device A ($L = 0.5 \mu\text{m}$ and $W = 400 \mu\text{m}$) than for device B ($L = 3 \mu\text{m}$ and $W = 70 \mu\text{m}$). We have also observed this trend of increasing transconductance with the decreasing gate length in

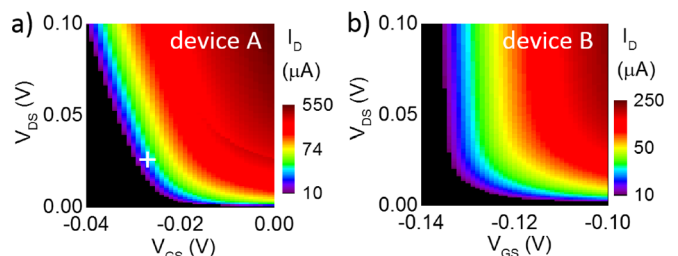


FIG. 2. HEMT DC transport at $T_{MC} < 100 \text{ mK}$ for (a) device A ($L = 0.5 \mu\text{m}$ and $W = 400 \mu\text{m}$) and (b) device B ($L = 3 \mu\text{m}$ and $W = 70 \mu\text{m}$), for mixing chamber temperature $T_{MC} \leq 100 \text{ mK}$, showing HEMT drain current (I_D) versus gate voltage V_{GS} and drain-source voltage V_{DS} . The white cross in (a) indicates the bias point for the data of Figs. 3(a)–3(c).

$T = 4$ K measurements of transistors of varying dimensions fabricated on the same wafer, where the total gate area was held approximately fixed. This observation provides a possible route for improving HEMT transconductance, and thus circuit gain, in future devices.

We next focus on characterization of the amplifier circuit for device A, as shown in Fig. 3, for which the HEMT is located on a separate die from the quantum dot and passives. For these measurements, the HEMT current is fed to a room temperature bias tee (Mini-Circuits model ZFBT-6GW+) with a low frequency cutoff of 0.1 MHz. The DC port of the bias tee is grounded, and the current at the RF port is further amplified by a room temperature current amplifier (Femto model HCA-10M-100K-C). For all data shown in Fig. 3, the quantum dot device is biased so that the resistance is roughly 100 k Ω , well above h/e^2 . The HEMT biasing point for Figs. 3(a)–3(c), $V_{GS} = -0.027$ V, $V_{DS} = 25$ mV, and $I_D = 22.3$ μ A, as indicated by the white cross in Fig. 2(a), is chosen for relatively low power dissipation (0.56 μ W), while maintaining a large DC transconductance (~ 5800 μ A/V).

The measured circuit gain versus frequency of dot device source voltage is shown in Fig. 3(a). From these data, the estimated 3 dB circuit bandwidth is 2.7 MHz. The origin of this bandwidth value is not currently understood and is an important topic of investigation for improvements in future devices. From the RC circuit formed by the dot device resistance, resistor R2, and the expected gate to source and drain capacitance from device geometry (~ 0.3 pF), we would optimistically predict a

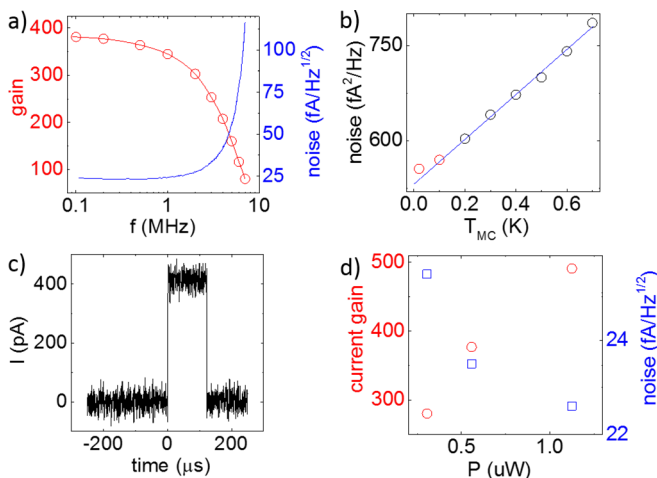


FIG. 3. Amplifier circuit characterization for device A. For (a)–(c), the HEMT biasing point is $V_{GS} = -0.027$ V, $V_{DS} = 25$ mV, and $I_D = 22.3$ μ A (0.56 μ W power dissipation), as indicated by the white cross in Fig. 2(a). For all measurements, the dot device resistance is set to ~ 100 k Ω . (a) Amplifier circuit current gain, referred to input current noise density versus frequency at $T_{MC} = 20$ mK. The open red circles are the measured gain, and the solid red line is a guide to the eye. The solid blue line is the measured current noise density. (b) Average spectral noise density from 0.1 to 1 MHz as a function of T_{MC} . The open circles indicate the measured values. The solid blue line is a linear fit to the black data points, measured above $T_{MC} = 200$ mK. Red points were excluded from the fit. (c) Dot current pulse measurement using homodyne detection at a dot source-drain voltage frequency of 1.4 MHz. (d) Amplifier current gain (red open circles), referred to input current noise density (blue open squares) at 0.2 MHz, versus HEMT power dissipation for $V_{DS} = 25$ mV.

3 dB bandwidth of nearly 10 MHz. Also from Fig. 3(a), at frequencies well below the 3 dB point, the circuit gain is ~ 380 . This is in contrast to the expected gain of ~ 580 which is estimated from the measured HEMT DC transconductance. We hypothesize that slow moving charge in the device, such as in the silicon doping layer or at the heterostructure surface/gate interface, may lead to this discrepancy.

Figure 3(a) also shows the measured current noise referred to amplifier input as a function of frequency. The majority of frequency dependence for these data can be explained using a white noise source, normalized by the gain when referred to amplifier input, although the origin of this noise is not known. At frequencies below 0.1 MHz, the circuit response is limited by the room temperature bias tee. Presumably, at very low frequencies, 1/f noise from both the HEMT and the quantum dot device should be observable. However, in the data of Fig. 3(a), hardly any 1/f character in the noise is visible. In comparison, for the noise performance of a similar HEMT circuit using a commercial off-the-shelf transistor (Broadcom ATF-36163),²⁴ a 1/f noise component can be clearly seen in the noise versus frequency spectrum, even for frequencies above 0.1 MHz. This suggests that the 1/f noise in our custom HEMT devices is relatively low. Observation of low 1/f noise in these devices may not be surprising, as the heterostructures were specifically designed for fabrication of quantum dot devices with low charge noise. In future devices, it may be possible to reduce the noise even further by using undoped heterostructures.^{30,31}

As can be seen in Fig. 3(b), the noise performance of the amplifier circuit benefits from operation at sub-Kelvin temperatures, with the noise continuing to decrease as T_{MC} is reduced down to ~ 0.1 K. As expected from Johnson noise due to resistive components, a nearly linear dependence of the noise spectral density on temperature is observed, as shown by the straight line fit in Fig. 3(b). For this fit, the two lowest temperature data points, below $T = 0.2$ K, are excluded. However, the divergence of the data from the straight line fit only appears below $T = 0.1$ K, suggesting that components contributing to the noise may be cooling below this temperature. This may not be completely surprising, as a Johnson noise contribution is expected from the quantum dot device and nichrome resistors R1 and R2, which are all located on a die separate from the HEMT, and thus may be able to cool to temperatures of ~ 100 mK. Considering only the Johnson noise from these components, we expect a slope of 220 fA²/Hz K, which is smaller than the slope of 350 fA²/Hz K obtained from the fit to the data. The origin of this excess noise is not known although we note that a similar trend of faster increase in noise versus temperature than that expected from simple Johnson noise was also seen for a similar amplifier circuit using commercial HEMTs.²⁴

In Fig. 3(c), we demonstrate the measurement of a current pulse through the quantum dot device using homodyne detection to emulate the detection of a single electron tunneling event. We apply a dot device source-drain voltage at a frequency of 2 MHz. The resulting current after amplification is mixed down to DC and filtered by a 1 MHz first order low pass RC filter. As an example, Barthel et al. find that for a quantum dot charge sensor in GaAs, the (0, 2) to (1, 1) charge transition for a nearby

double quantum dot can give rise to a change in dot conductance from nearly 0.3 to $0.1 e^2/h$, at an estimated optimal bias of 0.15 mV.¹⁸ For our circuit, with $R_2 \sim 100$ k Ω , this transition would give rise to a change in the current of ~ 390 pA. To mimic this signal, we apply a 400 pA rms current pulse through the dot device. Figure 3(c) shows the resulting output, as current referred to amplifier input. From the noise in the data, we find that the sensitivity of this measurement is 25 pA, giving a signal to noise ratio of ~ 16 , with a measured 10% to 90% rise time of ~ 0.5 μ s.

Achieving usable amplifier performance while maintaining as low of a power dissipation as possible is crucial to avoid heating of quantum dot devices. In Fig. 3(d), we show the amplifier gain and noise referred to input versus power dissipation, at a frequency of 0.2 MHz. The performance in terms of both noise and gain increases as the power consumption is increased up to ~ 1 μ W. The majority of small increase in noise as the power is lowered can be explained by an ~ 4 pA post amplifier noise source (this is the approximate expected noise contribution due to the room temperature current amplifier), normalized by the amplifier gain when referred to input. At the low power end, we find that for a power dissipation of 0.3 μ W, the current gain is 280 and the current noise density is 25 fA/Hz^{1/2}. In comparison, for the commercial HEMT model ATF-36163, a power consumption of roughly 10 μ W is required to achieve a single transistor stage gain of ~ 340 .²⁴ Interpolating between the two lowest power data points in Fig. 3(d), we predict a power consumption of only 0.46 μ W for this amount of gain, which is a reduction in power dissipation of more than a factor of 20 . We hypothesize that this relatively large gain at low power is achievable primarily due to the very high mobility of the channel supported by our heterostructure (peak mobility of $\sim 2 \times 10^6$ cm²/V s at 300 K).

Next, in Fig. 4, we investigate heating of a quantum dot device during operation of the HEMT for the fully integrated device “B,” where the HEMT, passives, and quantum dot are all located on the same die. Figure 4(a) shows the full width at half maximum of Coulomb blockade peaks in transport through the quantum dot device, as a function of mixing chamber temperature, where the HEMT power dissipation is set to a low value of 0.1 μ W. The open circles are measured data points, while the

solid red line is a straight line fit with the intercept at the origin to the data points above $T_{MC} \geq 0.3$ K. From the low temperature saturation of the peak width, we find a minimum quantum dot temperature of ~ 0.26 K. The limiting factor determining this base dot temperature is not known, but we note that for this measurement, the source voltage is applied to the dot via a stainless steel semi-rigid coax line with no filtering or attenuation.^{32,33} In principle, it should be possible to add cryogenic attenuators to this line to improve quantum dot electron temperature without any adverse effect on the performance of the amplifier circuit. Adding attenuation to both the HEMT source and drain coax lines is less straightforward since for the source line, this will decrease the output current and increase the impact of room temperature preamplifier noise on the total noise referred to input. However, the impact of noise on these lines on quantum dot temperature and the need for additional attenuation are not obvious. As for heating of the quantum dot due to power dissipation in the HEMT, the Coulomb blockade peak width did not appear to decrease significantly upon lowering the HEMT power dissipation from 0.1 to 0.05 μ W.

Figure 4(b) shows quantum dot temperature, as determined by the Coulomb blockade peak width, versus HEMT power dissipation. Significant heating of the quantum dot can be seen as the power is increased. However, for a power level of 0.56 μ W, we find a quantum dot temperature of 0.3 K, which is a rise of only 40 mK above the base dot temperature. We note that usable gain and noise levels can be achieved at even lower powers for device A (shorter channel HEMT with the improved gain). For example, a gain of ~ 290 and a noise level of 29 fA/Hz^{1/2} at 0.2 MHz can be obtained at a power level of 0.24 μ W. These results are promising, but further heating characterization after lowering of the dot base temperature will be necessary to determine ultimate performance. Improvements in heat sinking and thermal isolation of the dot from the HEMT may be necessary to ensure quantum dot cooling below 100 mK.

In conclusion, we have demonstrated integrated HEMT amplifiers operating at sub-Kelvin temperatures using high-mobility channels in GaAs/AlGaAs heterostructures. By fabricating custom transistors in these heterostructures, we are able to maintain gain while lowering power dissipation by more than an order of magnitude compared to a previous demonstration using a commercial off-the-shelf HEMT.²⁴ It may be possible to decrease power dissipation further through optimization of both HEMT geometry and heterostructure design. The amplifier shown here may be used with quantum dots in other material systems by mounting the GaAs die adjacent to the device and wire bonding. We expect that heating of the quantum dot device in this arrangement will be minimal, as it has been previously demonstrated that the use of an adjacent commercial HEMT amplifier circuit with a quantum dot device is compatible with dot electron temperatures of ~ 100 mK.³⁴ For the fully integrated device, here, we have demonstrated an on-chip amplifier and quantum dots in the GaAs/AlGaAs material system. However, a similar approach should be possible in other material systems supporting high mobility channels. In particular, for Si/SiGe heterostructures, integrated HEMT switches with quantum dots on the same die have already been demonstrated.³⁵

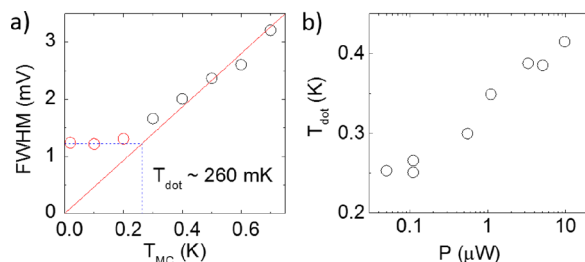


FIG. 4. Heating characterization for device B, where the HEMT and quantum dot are located on the same die. (a) Coulomb blockade peak width for the dot device versus T_{MC} for a HEMT power dissipation of 0.1 μ W. The estimated quantum dot temperature for this case is $T_{dot} \sim 260$ mK. (b) Quantum dot temperature, estimated from the measured Coulomb blockade peak width, versus HEMT power dissipation.

This work was performed at the Center for Integrated Nanotechnologies, a U.S. DOE, Office of Basic Energy Sciences user facility, and Sandia National Laboratories, a multimission laboratory managed and operated by National Technology and Engineering Solutions of Sandia LLC, a wholly owned subsidiary of Honeywell International Inc. for the U.S. Department of Energy's National Nuclear Security Administration under Contract No. DE-NA0003525. This paper describes objective technical results and analysis. Any subjective views that might be expressed in the paper do not necessarily represent the views of the U.S. Department of Energy or the United States Government.

REFERENCES

- ¹D. Loss and D. P. DiVincenzo, *Phys. Rev. A* **57**, 120 (1998).
- ²B. E. Kane, *Nature* **393**, 133 (1998).
- ³R. Hanson, L. P. Kouwenhoven, J. R. Petta, S. Tarucha, and L. M. K. Vandersypen, *Rev. Mod. Phys.* **79**, 1217 (2007).
- ⁴F. A. Zwanenburg, A. S. Dzurak, A. Morello, M. Y. Simmons, L. C. L. Hollenberg, G. Klimeck, S. Rogge, S. N. Coppersmith, and M. A. Eriksson, *Rev. Mod. Phys.* **85**, 961 (2013).
- ⁵D. D. Awschalom, L. C. Bassett, A. S. Dzurak, E. L. Hu, and J. R. Petta, *Science* **339**, 1174 (2013).
- ⁶M. Veldhorst, J. C. C. Hwang, C. H. Yang, A. W. Leenstra, B. de Ronde, J. P. Dehollain, J. T. Muhonen, F. E. Hudson, K. M. Itoh, A. Morello, and A. S. Dzurak, *Nat. Nanotechnol.* **9**, 981 (2014).
- ⁷J. T. Muhonen, A. Laucht, S. Simmons, J. P. Dehollain, R. Kalra, F. E. Hudson, S. Freer, K. M. Itoh, D. N. Jamieson, J. C. McCallum, A. S. Dzurak, and A. Morello, *J. Phys. Condens. Matter* **27**, 154205 (2015).
- ⁸E. Kawakami, T. Jullien, P. Scarlino, D. R. Ward, D. E. Savage, M. G. Lagally, V. V. Dobrovitski, M. Friesen, S. N. Coppersmith, M. K. A. Eriksson, and L. M. K. Vandersypen, *Proc. Natl. Acad. Sci. U. S. A.* **113**, 11738 (2016).
- ⁹J. M. Nichol, L. A. Orona, S. P. Harvey, S. Fallahi, G. C. Gardner, M. J. Manfra, and A. Yacoby, *npj Quantum Inf.* **3**, 3 (2017).
- ¹⁰J. Yoneda, K. Takeda, T. Otsuka, T. Nakajima, M. R. Delbecq, G. Allison, T. Honda, T. Kodera, S. Oda, Y. Hoshi, N. Usami, K. M. Itoh, and S. Tarucha, *Nat. Nanotechnol.* **13**, 102 (2018).
- ¹¹J. J. Pla, K. Y. Tan, J. P. Dehollain, W. H. Lim, J. J. L. Morton, F. A. Zwanenburg, D. N. Jamieson, A. S. Dzurak, and A. Morello, *Nature* **496**, 334 (2013).
- ¹²T. Nakajima, M. R. Delbecq, T. Otsuka, P. Stano, S. Amaha, J. Yoneda, A. Noiri, K. Kawasaki, K. Takeda, G. Allison, A. Ludwig, A. D. Wieck, D. Loss, and S. Tarucha, *Phys. Rev. Lett.* **119**, 017701 (2017).
- ¹³M. A. Broomer, T. F. Watson, D. Keith, S. K. Gorman, M. G. House, J. G. Keizer, S. J. Hile, W. Baker, and M. Y. Simmons, *Phys. Rev. Lett.* **119**, 046802 (2017).
- ¹⁴P. Harvey-Collard, B. D'Anjou, M. Rudolph, N. T. Jacobson, J. Dominguez, G. A. Ten Eyck, J. R. Wendt, T. Pluym, M. P. Lilly, W. A. Coish, M. Pioro-Ladrière, and M. S. Carroll, *Phys. Rev. X* **8**, 021046 (2018).
- ¹⁵J. M. Elzerman, R. Hanson, L. H. Willems van Beveren, B. Witkamp, L. M. K. Vandersypen, and L. P. Kouwenhoven, *Nature* **430**, 431 (2004).
- ¹⁶R. J. Schoelkopf, R. Wahlgren, A. A. Kozhevnikov, P. Delsing, and D. E. Prober, *Science* **280**, 1238 (1998).
- ¹⁷D. J. Reilly, C. M. Marcus, M. P. Hanson, and A. C. Gossard, *Appl. Phys. Lett.* **91**, 162101 (2007).
- ¹⁸C. Barthel, M. Kjærgaard, J. Medford, M. Stopa, C. M. Marcus, M. P. Hanson, and A. C. Gossard, *Phys. Rev. B* **81**, 161308R (2010).
- ¹⁹J. Stehlik, Y.-Y. Liu, C. M. Quintana, C. Eichler, T. R. Hartke, and J. R. Petta, *Phys. Rev. Appl.* **4**, 014018 (2015).
- ²⁰E. H. Visscher, J. Lindeman, S. M. Verbrugh, P. Hadley, J. E. Mooij, and W. van der Vleuten, *Appl. Phys. Lett.* **68**, 2014 (1996).
- ²¹S. L. Pohlen, R. J. Fitzgerald, J. M. Hergenrother, and M. Tinkham, *Appl. Phys. Lett.* **74**, 2884 (1999).
- ²²I. T. Vink, T. Nooitgedagt, R. N. Schouten, L. M. K. Vandersypen, and W. Wegscheider, *Appl. Phys. Lett.* **91**, 123512 (2007).
- ²³M. J. Curry, T. D. England, N. C. Bishop, G. Ten-Eyck, J. R. Wendt, T. Pluym, M. P. Lilly, S. M. Carr, and M. S. Carroll, *Appl. Phys. Lett.* **106**, 203505 (2015).
- ²⁴L. A. Tracy, D. R. Luhman, S. M. Carr, N. C. Bishop, G. A. Ten-Eyck, T. Pluym, J. R. Wendt, M. P. Lilly, and M. S. Carroll, *Appl. Phys. Lett.* **108**, 063101 (2016).
- ²⁵D. J. Reilly, *npj Quantum Inf.* **1**, 15011 (2015).
- ²⁶D. P. DiVincenzo, and IBM, *Fortschr. Phys.* **48**, 771 (2000).
- ²⁷T. D. Ladd, F. Jelezko, R. Laflamme, Y. Nakamura, C. Monroe, and J. L. O'Brien, *Nature* **464**, 45 (2010).
- ²⁸F. Martins, F. K. Malinowski, P. D. Nissen, E. Barnes, S. Fallahi, G. C. Gardner, M. J. Manfra, C. M. Marcus, and F. Keummeth, *Phys. Rev. Lett.* **116**, 116801 (2016).
- ²⁹T. Hensgens, T. Fujita, L. Janssen, X. Li, C. J. Van Diepen, C. Reichl, W. Wegscheider, S. Das Sarma, and L. M. K. Vandersypen, *Nature* **548**, 70 (2017).
- ³⁰S. Mondal, G. C. Gardener, J. D. Watson, S. Fallahi, A. Yacoby, and M. J. Manfra, *Solid State Commun.* **197**, 20 (2014).
- ³¹S. Fallahi, J. R. Nakamura, G. C. Gardner, M. M. Yannell, and M. J. Manfra, *Phys. Rev. Appl.* **9**, 034008 (2018).
- ³²J. M. Martinis and M. Nahum, *Phys. Rev. B* **48**, 18316 (1993).
- ³³D. Vion, P. F. Orfila, P. Joye, D. Esteve, and M. H. Devoret, *J. Appl. Phys.* **77**, 2519 (1995).
- ³⁴T. Knapp, J. P. Dodson, B. Thorggrimsson, D. E. Savage, M. Lagally, S. Coppersmith, and M. A. Eriksson, in APS March Meeting, 2018.
- ³⁵D. R. Ward, D. E. Savage, M. G. Lagally, S. N. Coppersmith, and M. A. Eriksson, *Appl. Phys. Lett.* **102**, 213107 (2013).